Monthly Notices
of the
ROYAL ASTRONOMICAL SOCIETY

MNRAS **457,** 2951–2957 (2016) doi:10.1093/mnras/stw165

Detection of a second high-velocity component in the highly ionized wind from PG 1211+143

Ken Pounds,[1]★ Andrew Lobban,[1] James Reeves[2] and Simon Vaughan[1]

[1]*Department of Physics and Astronomy, University of Leicester, Leicester LE1 7RH, UK*
[2]*School of Physical Sciences, Keele University, Keele ST5 5BG, UK*

Accepted 2016 January 18. Received 2015 December 22; in original form 2015 July 28

ABSTRACT

An extended *XMM–Newton* observation of the luminous narrow line Seyfert galaxy PG1211+143 in 2014 has revealed a more complex highly ionized, high-velocity outflow. The detection of previously unresolved spectral structure in Fe K absorption finds a second outflow velocity component of the highly ionized wind, with an outflow velocity of $v \sim 0.066 \pm 0.003c$, in addition to a still higher velocity outflow of $v \sim 0.129 \pm 0.002c$ consistent with that first seen in 2001. We note that chaotic accretion, consisting of many prograde and retrograde events, offers an intriguing explanation of the dual velocity wind. In that context the persisting outflow velocities could relate to physically distinct orientations of the inner accretion flow, with prograde accretion yielding a higher launch velocity than retrograde accretion in a ratio close to that observed.

Key words: galaxies: active – galaxies: individual: PG1211+143 – quasars: general – galaxies: Seyfert – X-rays: galaxies.

1 INTRODUCTION

X-ray spectra from an *XMM–Newton* observation of the luminous Seyfert galaxy PG1211+143 in 2001 provided the first detection in a non-BAL (broad absorption line) active galactic nucleus (AGN) of strongly blue-shifted absorption lines of highly ionized gas, corresponding to a sub-relativistic outflow velocity of $\sim 0.09c$ (Pounds et al. 2003). That velocity was based primarily on the identification of a strong absorption line at ∼7 keV with the resonance Lyman α transition in Fe XXVI. The subsequent inclusion of additional absorption lines, of Ne, Mg, Si and S, led to the re-identification of the ∼7 keV absorption line with the resonance 1s–2p transition in Fe XXV, and a revised outflow velocity of $0.14 \pm 0.01c$ (Pounds & Page 2006). Further observations of PG1211+143 over several years with *XMM–Newton*, *Chandra* and *Suzaku* found the high-velocity outflow to be persistent but of variable strength (Reeves et al. 2008). Evidence that the mean outflow in PG1211+143 was both massive and energetic – with potential importance for galaxy feedback – was obtained from the detection of P Cygni and other broad emission features by combining the 2001, 2004 and 2007 *XMM–Newton* European Photon Imaging Camera (EPIC) spectra (Pounds & Reeves 2009).

Examination of archival data from *XMM–Newton* and *Suzaku* subsequently showed ultrafast, highly ionized outflows (UFOs) to be relatively common in nearby, luminous AGN (Tombesi et al. 2010, 2011; Gofford et al. 2013). The frequency of these detections appeared to confirm a substantial covering factor, with a persistent wind having sufficient mechanical energy to disrupt the bulge gas in the host galaxy (Pounds 2014a). An indication how much of that energy could be lost before reaching a still-active star forming region came with evidence of a UFO shocking against the interstellar medium or slower moving ejecta in the low-mass Seyfert galaxy NGC 4051 (Pounds & Vaughan 2011; Pounds & King 2013).

Determination of the correct wind velocity, v, is critically important in estimating the mass and energy rates of AGN winds, with the latter being dependent on v^3 in a radial outflow. However, significant uncertainty remains when the deduced velocity depends on the identification of a single blue-shifted absorption line, typically of Fe K, as in many early UFO detections (e.g. Tombesi et al. 2010). Spectral modelling over a wider energy band reduces ambiguities in line identification, as first demonstrated in Pounds & Page (2006), while also providing additional outflow parameters, including the mean ionization parameter and column density. Such broad-band spectral modelling was used in the second paper on the *XMM–Newton* archival data (Tombesi et al. 2011) and by Gofford et al. (2013) in their similar analysis of *Suzaku* data.

In this paper, we make a further addition, in simultaneously modelling the outflow of PG1211+143 with both photoionized absorption and emission grids. To quantify absorption and emission structure, we employ photoionized grids of pre-computed spectra based on the XSTAR code (Kallman et al. 1996), with the publicly available grid 25 (turbulence velocity 200 km s^{-1}) being found to provide a satisfactory match to the highly ionized absorption, and velocity-broadened emission adequately modelled by grid 22 (turbulence velocity 3000 km s^{-1}).

★ E-mail: kap@le.ac.uk

Initially employing that procedure in re-modelling the 2001 outflow, we re-affirm a column density $N_{\rm H}$ of $\sim 10^{23}$ cm^{-2}, ionization parameter logξ $\sim$ 2.9 erg cm s^{-1} and outflow velocity $v \sim 0.14 \pm 0.01c$. By comparison with the typical properties of UFOs (Tombesi et al. 2011) and with the new observations reported here, it appears the unusually low outflow ionization – and correspondingly high opacity – in the 2001 observation was a primary reason for it being amongst the most highly visible UFOs yet seen.

2 A NEW *XMM–NEWTON* OBSERVATION OF PG1211+143 IN 2014

In order to further explore the ionized wind in PG1211+143, an extended *XMM–Newton* observation was carried out during seven spacecraft orbits over the period 2014 June 2 to 2014 July 9. This paper describes the analysis of high-energy spectral data, with subsequent papers reporting the detection of a low-ionization outflow in the soft X-ray spectrum, and evidence for short-term variability. We use data from the EPIC-pn CCD (Strueder et al. 2001), operated in large window mode.

On-target exposures for individual orbits were typically $\sim$100 ks, apart from the fifth observation (rev2664) of $\sim$55 ks, giving a total on-target exposure of $\sim$630 ks. Full details of the *XMM–Newton* observing log and data extraction procedures, and of accompanying *Swift* observations, are given in Lobban et al. (2016), reporting the results of a detailed timing analysis.

Raw data were processed using version 14.0 of the *XMM–Newton* Scientific Analysis Software[1] package, following standard procedures. Source events were extracted from 20 arcsec circular regions centred on the AGN, while background events were taken from much larger regions away from the target source and from other nearby background sources. For our EPIC-pn analysis, we utilized single and double good pixel events (PATTERN $\leq$ 4). The exclusion of short intervals of background flaring resulted in a final $\sim$570 ks of high-quality pn data. The total residual background count rate was $<$1 per cent of the source rate for all three EPIC cameras in each observation (Fig. 1).

We assume an AGN redshift of $z = 0.0809$ (Marziani et al. 1996). Spectral modelling is based on the XSPEC package (Arnaud 1996) and includes absorption due to the line-of-sight Galactic column of $N_{\rm H} = 2.85 \times 10^{20}$ cm^{-2} (Murphy et al. 1996). 90 per cent confidence intervals on model parameters are based on $\Delta\chi^2 = 2.706$. Published estimates for the black hole mass in PG1211+143 range from 3×10^7 M$_\odot$ (Kaspi et al. 2000) to 1.5×10^8 M$_\odot$ (Bentz et al. 2009), with the lower value making the mean luminosity close to the Eddington limit. All derived velocities are corrected for the relativistic Doppler effect.

3 CONFIRMATION OF A HIGH-VELOCITY WIND IN PG1211+143

While examination of pn spectra from the seven individual orbits in 2014 showed strong variability in the soft X-ray band, the harder continuum changes relatively little above $\sim$2 keV. To obtain a baseline hard X-ray spectrum of PG1211+143 with maximum statistical quality we therefore summed low background pn data from all seven orbits for an initial spectral analysis. The resulting low background source exposure is a factor $\sim$10 greater than for any of the previous *XMM–Newton* observations in 2001, 2004 and 2007.

[1] http://xmm.esac.esa.int/sas/

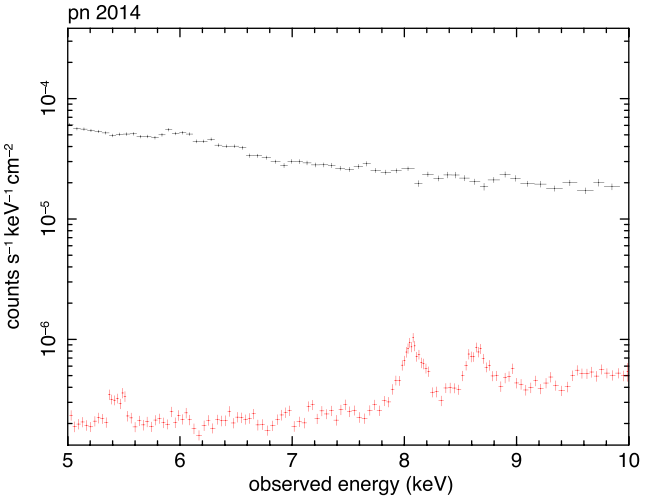

Figure 1. Comparison of the source (black) and background spectra (red) for the stacked 2014 pn data. The source spectrum is plotted without background subtraction and is near identical to that including background subtraction, confirming the Fe K absorption features are not due to fluorescent Cu and Zn lines from the detector structure.

Fig. 2 compares the stacked pn spectrum from 2014 with that from 2001, both data sets being plotted as a ratio to a double power-law continuum of photon index $\Gamma \sim 1.6$ and $\Gamma \sim 3$ to match a variable 'soft excess' at the lowest energies. Visual comparison of the two plots confirms that emission and absorption features are significantly better defined in the longer 2014 exposure. The emission near 6 keV is now resolved into low- and high-ionization components, and the prominent absorption line at $\sim$7 keV is again seen in the 2014 data, albeit being less deep than in 2001. Other differences in the 2014 spectrum include weaker absorption in the lower mass ions, but a clear indication of additional absorption structure in the Fe K band between 6–10 keV. Those differences suggest the fast wind in 2014 was more highly ionized than in 2001, a suggestion we now confirm by modelling the broad-band spectrum from 2014 with the same photoionized grids used to parametrize the 2001 outflow.

Fig. 3 (top panel) shows a section of the stacked pn spectrum covering the Fe K region. The data have been grouped with a minimum of 25 counts (for χ^2 compatibility) and with a maximum of three data points per pn camera resolution (full width at half-maximum) to optimize the visibility of spectral structure. The emission near 6 keV is resolved into components with rest energies close to the neutral Fe K fluorescent emission line and the 1s–2p resonance emission lines of He-like and H-like Fe, respectively. The absorption line at $\sim$7 keV is a factor $\sim$3 weaker than the corresponding line in 2001, with an equivalent width (EW) of 37 $\pm$ 5 eV. In contrast, the deep 2014 exposure reveals additional structure at $\sim$6–10 keV, with apparent absorption lines at $\sim$6.9, $\sim$7.3, $\sim$7.5, $\sim$7.8, $\sim$8.2 and $\sim$8.6 keV.[2]

[2] The absorption lines at $\sim$8.2 and $\sim$8.6 keV lie close to fluorescent X-ray emission lines of Cu and Zn arising from energetic particle impacts on the pn camera electronics board (Strueder et al. 2001). Fortunately, the low particle background throughout most of the 2014 *XMM–Newton* observations (Fig. 1) ensured such background features have a negligible effect on the source spectrum, an outcome confirmed by obtaining a very similar ratio plot to that in Fig. 3 when no background data is subtracted.

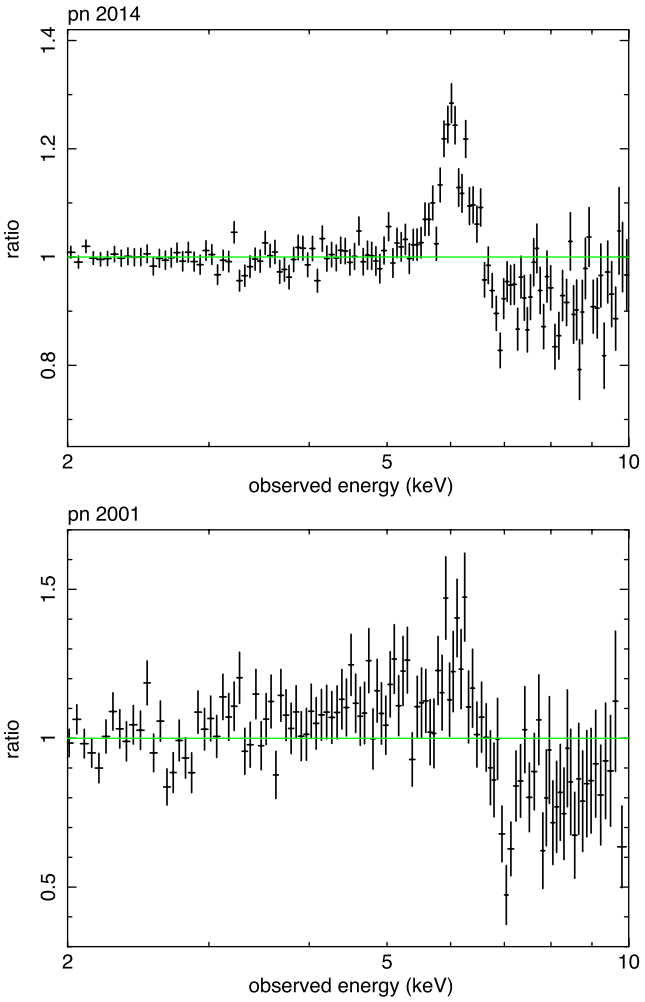

Figure 2. Comparison of the stacked pn data from the 2014 observation of PG1211+143 with that from the 2001 observation, both plotted as a ratio to a double power-law continuum. While the most prominent absorption line near 7 keV is weaker than in 2001, the much longer 2014 exposure allows the overall spectrum to be better defined. In particular, the Fe K emission profile is resolved into high- and low-ionization components and additional absorption structure is indicated at higher energies.

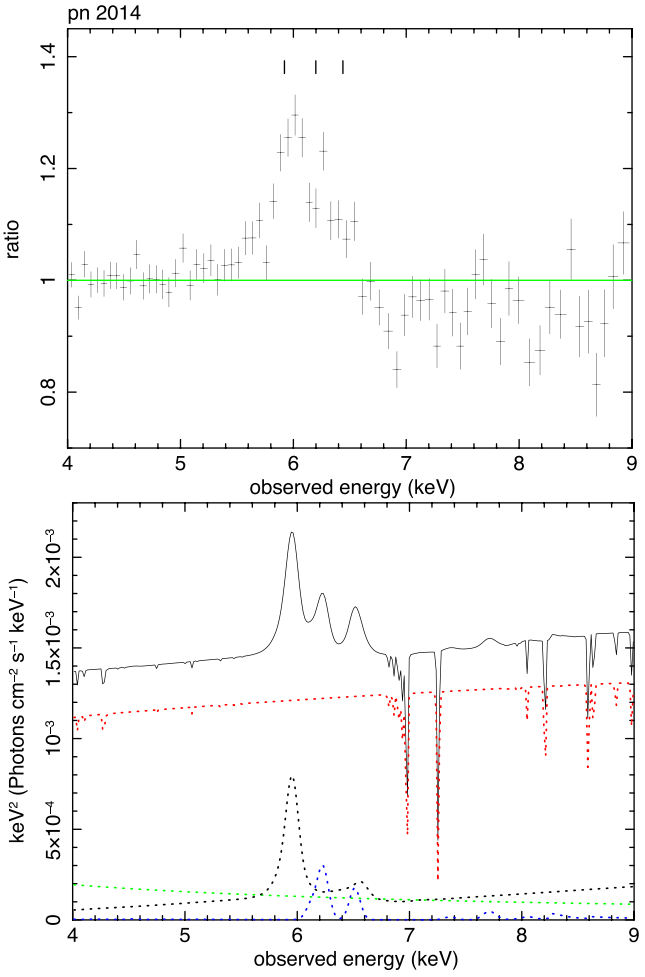

Figure 3. (top) Spectral structure in the stacked 2014 pn spectrum from Fig. 2 resolves Fe K emission components corresponding to the Fe K fluorescence line and resonance emission from Fe XXV and Fe XXVI ions. (lower) The addition of photoionized emission and absorption spectra match the resonance emission lines observed at ∼6.2 and ∼6.45 keV, with photoionized absorption imprinted on the hard power-law continuum (red). A single outflow velocity identifies absorption lines at ∼7.0, ∼7.3, ∼8.2 and ∼8.6 keV with the α and β lines, again of Fe XXV and Fe XXVI. The model includes continuum reflection and linked Fe K fluorescence line emission (black) and is completed with a softer, unabsorbed power law (green) required by interorbit difference spectra (see text).

Gaussian fitting of those spectral features is detailed in Section 4.1, and while the significance of individual lines is limited, we emphasize that finding a common velocity for a line series can be highly significant, again underlining the importance of taking proper account of multiple absorption lines in the study of X-ray outflows. Analysis and interpretation of the Fe K absorption line structure, providing further detail on the highly ionized wind in PG1211+143, is the main purpose of this paper.

Before testing for ionized absorption, it is especially important to correctly model the underlying continuum for such high-quality data. In particular, scattering from optically thick matter (or so-called reflection found to be common in AGN spectra; Nandra & Pounds 1994) may impose a step change near the Fe K absorption edge (∼6.5 keV in observer space), and an indication of such an effect can be seen in Fig. 3 (top panel). To quantify that 'reflection', we added a XILLVER component (Garcia et al. 2013) to the power-law continuum model in XSPEC, simultaneously matching the fluorescent Fe K emission line and continuum reflection from optically thick-ionized matter. When previously modelled with a Gaussian, the Fe K line energy of ∼5.96 keV (∼6.44 keV at the AGN redshift), and EW of 73 eV yielded a 2–10 keV spectral fit statistic of (χ^2_ν of 1513/1364). Re-fitting the Gaussian with XILLVER provided a corresponding adjustment to the continuum from reflection, with a further improvement in χ^2_ν of 1495/1364. The reflection component had an ionization parameter of logξ ∼ 2.1, with inclination fixed at 45° and a small outflow velocity of 1500 ± 1200 km s^{-1} in the AGN rest-frame. Critically, although reduced in depth, the absorption features at ∼7–9 keV in Fig. 3 (top) remained clearly visible.

Having modelled the underlying continuum, a photoionized absorber was then added to match that absorption structure, obtaining a significant improvement to the spectral fit (χ^2_ν of 1470/1361), for a column density $N_{\rm H}$ of 7.2 ± 5.0 × 10^{22} cm^{-2}, ionization parameter logξ = 3.3 ± 0.1 erg cm s^{-1} and outflow velocity of 0.119 ± 0.003c. The addition of a photoionized emission spectrum, with tied ionization parameter, reproduced the ionized emission lines at ∼6.2 and ∼6.45 keV, and further improved the fit (χ^2_ν of 1445/1359), with

the column density of the absorber decreasing to N_H of $5.8 \pm 3.2 \times 10^{22}$ cm^{-2}. The tied ionization parameter (logξ = 3.42 ± 0.05 erg cm s^{-1}) and absorber velocity were unchanged in this second fit, while untying the ionization parameters of the emission and absorption spectra made little difference to χ^2. The ionized emission spectrum was found to have a blueshift (relative to the AGN), corresponding to an outflow velocity of 4200 ± 1200 km s^{-1}, which we take to represent a mean value averaged over an extended ionized outflow.

Fig. 3 (lower panel) illustrates the key 4–9 keV section of the single velocity outflow model, with absorption lines seen in the data at ∼7 and ∼7.3 keV identified with the 1s–2p resonance lines of Fe XXV and Fe XXVI, and absorption lines at ∼8.2 and ∼8.6 keV with Heβ and a blend of Lyman β and Heγ of the same ions. Finding a match to four absorption features with the same outflow velocity adds confidence in the robustness of the spectral fit.

The photoionized emission spectrum in Fig. 3 correspondingly matches the two high-energy components in the ratio plot, being identified with the He- and H-like resonance lines, in a ratio set by the linked ionization parameter. Encouragingly, the Heβ emission line can also be seen at ∼7.7 keV in both data and model, with a similar blueshift.

3.1 A second velocity component in the highly ionized wind of PG1211+143

Examination of Fig. 3 shows that while the absorption lines seen at ∼7, ∼7.3, ∼8.2 and ∼8.6 keV are matched by resonance and higher order transitions in Fe XXV and Fe XXVI in the photoionized outflow, the comparison of model and data is incomplete. To seek a further improvement in the fit a second absorber was therefore added, with ionization parameter, column density and velocity again free. Re-fitting the 2–10 keV spectrum showed a further substantial improvement to the fit (χ^2_ν of 1415/1356), with the second absorption component having a significantly lower outflow velocity of $0.066 \pm 0.003c$.

Fig. 4 (top) illustrates the dual velocity absorber model, with the Lyman α line of the lower velocity flow now blending with Heα from the high-velocity wind to provide a better match to the broad absorption feature observed at ∼6.9 keV. A consequence of that line blend is to increase the relative strength of the higher velocity Lyman α line and hence – substantially – both the ionization parameter and column density of that flow component. The higher outflow velocity is also increased slightly in the dual velocity fit, to $0.129 \pm 0.002c$.

An important consequence of simultaneously modelling the absorption and (re-)emission spectra is demonstrated by the Heα absorption line in the lower velocity outflow, previously partly hidden by the emission line at ∼6.5 keV. In turn, the partial absorption of the Fe Lyman α emission line explains the relative weakness of that emission component in the data ratio plot. Comparing Figs 3 and 4, and the fit residuals, confirms that a significant contribution to the improved dual absorber fit lies in better matching the observed opacity at ∼7 keV, while the lower velocity He-like absorption line models the sharp drop in the data at ∼6.6 keV as it cuts into the blue wing of the H-like emission line.

From the dual velocity outflow spectral fit, we find a mean 2–10 keV source luminosity of $\sim 6 \times 10^{43}$ erg s^{-1}. The total extracted (absorbed) and added (emission) luminosities are $\sim 2.2 \times 10^{42}$ erg s^{-1} and $\sim 7 \times 10^{41}$ erg s^{-1}, respectively, with the lower velocity, lower ionization absorber contributing ∼80 per cent of the 2–10 keV opacity. Table 1 summarizes the main parameters of the

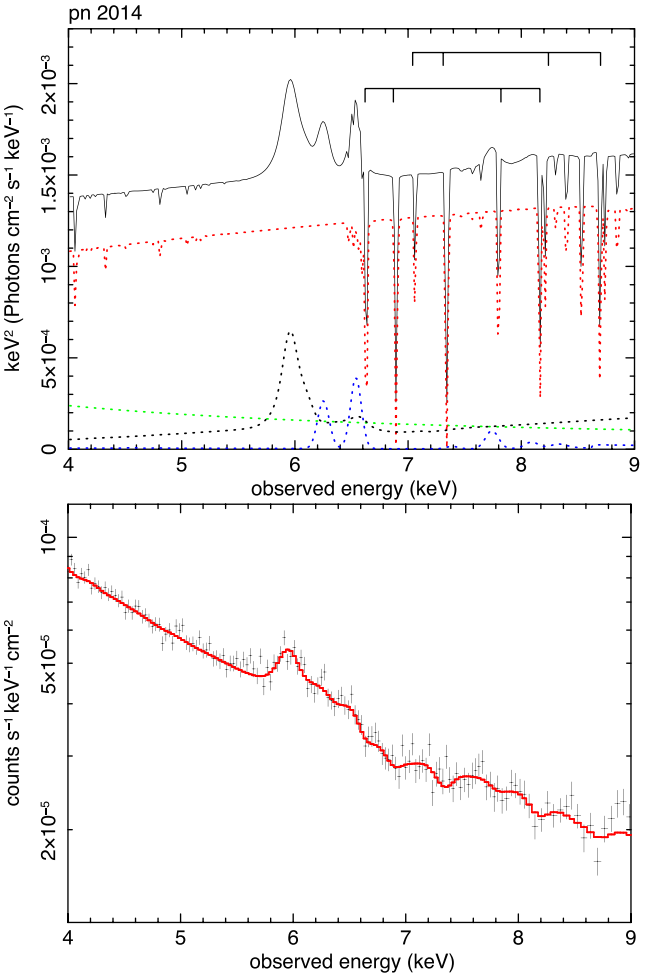

Figure 4. Comparison of stacked pn data and the final outflow model fit including a second highly ionized absorption component. (top) The principal emission and absorption lines in the two-component absorber model now provide a good match to spectral features in the data. Colour coding of the emission lines includes black for the fluorescent Fe K line, and blue for the high-ionization emission. The hard power-law and unabsorbed power-law components are shown in red and green, respectively. Separate absorption line sequences of Lyman α, Heα, Lyman β and Heβ for outflow velocities of $\sim 0.066c$ and $\sim 0.129c$ are marked on the plot. (lower) While lacking the visual clarity of a similar plot obtained with higher resolution spectra data, individual emission and absorption features remain visible when folded through the CCD response function.

Table 1. Final parameters of the highly ionized outflow obtained from a 2–10 keV spectral fit to the 2014 pn data, with two photoionized absorbers, defined by ionization parameter ξ (erg cm s^{-1}), column density N_H (cm^{-2}) and outflow velocity (v/c), together with a photoionized emission spectrum modelled by an ionization parameter and outflow velocity. Extracted or added luminosities (erg s^{-1}) over the fitted spectral band 2–10 keV and the improvement in χ^2 are also given for each photoionized model component.

Comp	logξ	$N_H(10^{23})$	v/c	$L_{abs/em}$	$\Delta\chi^2$
abs	4.0 ± 0.2	3.7 ± 2.9	0.129 ± 0.002	5×10^{41}	15/3
abs	3.4 ± 0.1	2.0 ± 1.0	0.066 ± 0.003	1.8×10^{42}	27/3
emi	3.5 ± 0.1	1 (f)	0.011 ± 0.003	7×10^{41}	34/3

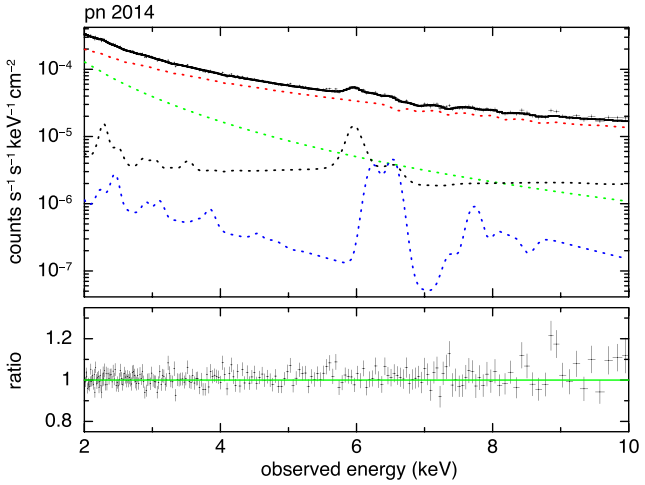

Figure 5. (top) Comparison of the dual velocity outflow model and pn data over the full 2–10 keV band, showing the individual spectral components, with the power law and reflection continua (red, green and black), the fluorescent Fe K (also black) and ionized emission lines (blue).

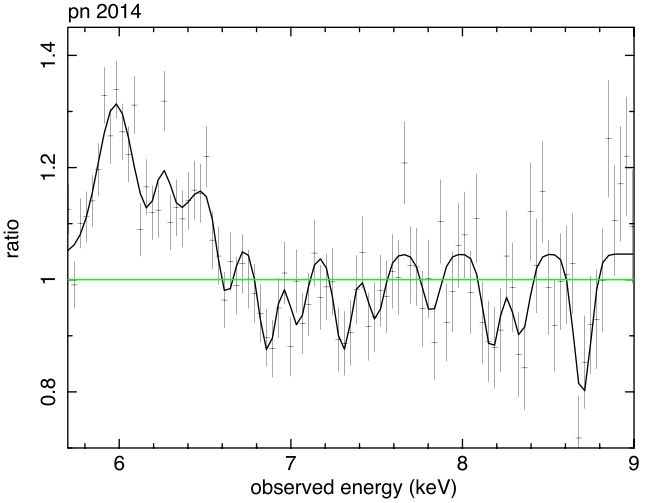

Figure 6. Gaussian line fitting to spectral structure in the stacked pn data from the *XMM–Newton* observation of PG1211+143 in 2014. In this plot, data binning has been relaxed with the removal of the limit of three data points per resolution element to provide smoother Gaussian profiles. Nine possible absorption lines are detected, numbered from left to right as abs1–abs 9 in Table 2, where the measured energy, proposed identification and outflow velocity are listed.

photoionized absorption and emission spectra describing the highly ionized outflow in PG1211+143 in 2014.

To summarize, in XSPEC terms the final model is TBabs($\mathrm{pl_{soft}}$ + ($\mathrm{pl_{hard}}$)(mtable)(mtable) + XILLVER + atable), where $\mathrm{pl_{hard}}$ is the dominant continuum component ($\Gamma \sim 1.6$), subject to ionized absorption from the two outflow components. XILLVER represents the reflection continuum and associated Fe K fluorescence line, as described in the text. $\mathrm{pl_{soft}}$ is a soft continuum component ($\Gamma \sim 2.9$) found from interorbit difference spectra where the subtraction of low flux spectra from high flux spectra show the residual spectrum is well described by a simple power law. While this variable, soft continuum component has little impact on the present analysis, it is included for consistency with the soft X-ray analysis of *XMM–Newton* grating spectra (Pounds et al. 2015).

Fig. 4 (lower panel) compares the stacked 2014 pn data with the dual velocity outflow model (plotted immediately above), while Fig. 5 shows the spectral model plot over the full 2–10 keV energy range to better illustrate continuum and line emission components.

From the lower panel of Fig. 5, we note the absence of a hard excess in the data-to-model ratio confirms that continuum reflection is adequately modelled by XILLVER, at least up to 10 keV in our spectral fit, and does not indicate the strong reflection reported in Zoghbi et al. (2015). Although discussed further at this point, we note the strongest residual in the lower part of Fig. 5 is excess emission near 9 keV, which – if confirmed – could represent blue-shifted Fe XXVI radiative recombination continuum (RRC), perhaps indicative of a cooling flow.

4 SUPPORTING EVIDENCE FOR DUAL OUTFLOW VELOCITIES

4.1 Gaussian line fitting to the observed spectral structure

Gaussian fitting to the emission and absorption line structure seen in the stacked pn data provides a model-independent check on the robustness of the above spectral analysis. The 4–10 keV ratio plot shown in Fig. 6, obtained by removing the photoionized absorption and emission spectra from the best-fitting model of Section 3, was scanned sequentially with positive and negative Gaussians, having a minimum (1σ) line width of 50 eV comparable to the pn detector resolution. All features giving $\Delta\chi^2 \gtrsim 6$ were recorded and the sweep was then repeated with two broader absorption features at ~7 keV and ~8.2 keV re-fitted as narrow line pairs, making nine absorption lines in all. The emission and absorption blend at ~6.5–6.6 keV was resolved by fixing the emission line width at 100 eV. The resulting fit is shown in Fig. 6, with the measured line energies, EW and proposed identifications listed in Table 2.

Of the nine narrow absorption lines in Table 2, those at ~6.62, ~6.87, ~7.82 and ~8.17 keV have observed line energies consistent with an outflow velocity in the range 0.065–0.069c when identified with the α and β lines of Fe XXV and Fe XXVI. Taken as a line set, the weighted mean velocity is $0.067 \pm 0.001c$ and the combined significance is high ($\Delta\chi^2 = 51/8$), providing strong model-independent support for the lower velocity absorber in Table 1. Four (of five) remaining Gaussians, at ~7.04, ~7.31, ~8.34 and ~8.70 keV, are consistent with the higher outflow velocity found in spectral modelling, with individual values – based on identification with the same set of resonance absorption lines – ranging from 0.125–0.134c, and a mean value $v \sim 0.128 \pm 0.002c$. For this higher velocity line-set the statistical improvement of Gaussian line fitting is also highly significant ($\Delta\chi^2 = 57/8$). Absorption line 5 does not fit the dual outflow velocity pattern, but is interesting in that the possible association with the Fe XXV resonance line would match a third outflow velocity of $v \sim 0.19c$ which gave a marginal improvement to the dual velocity spectral modelling described in Section 3.2.

5 DISCUSSION

The extended observation of PG1211+143 in 2014 has provided high-quality hard X-ray spectra revealing previously unseen spectral structure of a UFO in the ~6–10 keV energy band. Spectral modelling has identified the observed absorption structure with resonance and higher order lines of highly ionized Fe, consistent with two distinct outflow velocities. The faster wind component has a velocity of $v \sim 0.13c$, similar to that first seen in 2001, but with a higher column density and ionization parameter. The second

Table 2. Sequential Gaussian fits to the positive and negative features in the pn 2014 data shown in Fig. 6. Absorption lines (abs 1–9) have a fixed width comparable to the pn detector resolution, with the fitted line energy, proposed identification and corresponding outflow velocity listed in each case. Improvement in $\Delta\chi^2$ is after re-fitting the data at 4–10 keV following each added line. All line identifications are with transitions in Fe XXV or Fe XXVI. The EW of each line has been estimated separately in XSPEC.

Component	Obs energy (keV)	EW (eV)	Rest energy (keV)	Line id	Energy (keV)	v/c	$\Delta\chi^2$
Fe K α	5.98 ± 0.01	80 ± 7	6.46 ± 0.01	Fe K α	6.40	0.009 ± 0.002	139/3
Fe 25	6.26 ± 0.02	19 ± 7	6.77 ± 0.02	Heα	6.70	0.010 ± 0.003	8/2
Fe 26	6.49 ± 0.07	73 ± 15	7.02 ± 0.07	Ly α	6.96	0.01 ± 0.01	34/2
abs 1	6.62 ± 0.02	−31 ± 11	7.16 ± 0.02	Heα	6.70	0.066 ± 0.003	12/2
abs 2	6.87 ± 0.01	−22 ± 6	7.43 ± 0.01	Ly α	6.96	0.065 ± 0.002	16/2
abs 3	7.04 ± 0.02	−11 ± 7	7.61 ± 0.02	Heα	6.70	0.127 ± 0.003	7/2
abs 4	7.31 ± 0.02	−22 ± 8	7.90 ± 0.02	Ly α	6.96	0.126 ± 0.003	25/2
abs 5	7.49 ± 0.03	−9 ± 7	8.10 ± 0.03	Heα	6.70	0.188 ± 0.004	7/2
abs 5	7.49 ± 0.03	−9 ± 7	8.10 ± 0.03	Ly α	6.96	0.151 ± 0.004	7/2
abs 6	7.82 ± 0.03	−16 ± 9	8.45 ± 0.03	Heβ	7.88	0.069 ± 0.003	10/2
abs 7	8.17 ± 0.02	−20 ± 8	8.83 ± 0.02	Ly β	8.25	0.068 ± 0.002	13/2
abs 8	8.34 ± 0.04	−16 ± 9	9.02 ± 0.04	Heβ	7.88	0.134 ± 0.005	6/2
abs 9	8.70 ± 0.02	−41 ± 11	9.40 ± 0.02	Ly β	8.25	0.129 ± 0.003	19/2
abs 9	8.70 ± 0.02	−41 ± 11	9.40 ± 0.02	Heγ	8.29	0.125 ± 0.003	19/2

outflow component, not resolved in the EPIC data in 2001, has a similar column density but a lower velocity $v \sim 0.066c$.

Key factors in identifying the lower velocity flow in 2014 were the high quality of the stacked 2014 spectral data, allowing spectral features to be identified near the limit of CCD energy resolution, and the simultaneous modelling of highly ionized emission, which allowed – in particular – the lower velocity Fe XXV He-α absorption line to be detected. The photoionized emission spectrum also successfully reproduces the higher energy features observed in the stacked 2014 pn data, identified with resonance emission from He- and H-like Fe ions in a similar ratio to that seen in absorption. Comparison of absorbed and (re-) emission luminosities indicates a substantial covering factor of the highly ionized wind.

An important outcome of the present analysis is in finding that the ultrafast outflow discovered in an *XMM–Newton* observation in 2001 is again detected in 2014. Although not resolved in the Fe K spectrum in 2001, there is independent evidence for the co-existence of the lower velocity outflow in that earlier observation, from a re-analysis of the soft X-ray spectrum (Pounds 2014b) and in an earlier partial-covering spectral fit which required an absorber moving at $\sim$0.07c to explain continuum curvature (Pounds & Reeves 2009).

The properties of powerful AGN winds are reviewed in King & Pounds (2015), where a highly ionized wind is envisaged being launched at the local escape velocity by continuum photons from a SMBH accreting at modest Eddington ratios $\dot{m} = \dot{M}/\dot{M}_{\rm Edd} \sim 1$, finding – for accretion from a disc – the excess accreting matter is expelled in a quasi-spherical wind, with a launch velocity $v \simeq \frac{\eta}{\dot{m}}c \sim 0.1c$. Observational support for that picture is provided by recent archival searches (Tombesi et al. 2010, 2011; Gofford et al. 2013) which find a substantial fraction of luminous AGN having a highly ionized wind with a velocity in the range $\sim$0.03–0.3c

The new observations indicate a more complex picture, with two distinct outflow velocities, co-existing in observations 13 years apart. Chaotic accretion (King & Pringle 2006), consisting of many prograde and retrograde events, offers an intriguing explanation of such a dual velocity wind, the persistence of two distinct outflow velocities perhaps relating to physically distinct orientations of the inner accretion flow, both close to Eddington, and with differing values of the accretion efficiency η and hence of velocity. That possibility is discussed in more detail by King & Nixon (in preparation).

Higher resolution hard X-ray spectra from the forthcoming *Astro-H* observatory should show how common are such complex highly ionized AGN winds as reported here for PG1211+143.

6 CONCLUSION

An extended *XMM–Newton* observation of the luminous narrow line Seyfert galaxy PG1211+143 in 2014 has revealed previously unseen spectral structure in Fe K absorption, finding a second high-velocity component of the highly ionized wind. In identifying that additional complexity within the limits of CCD energy resolution, the 2014 observation benefited critically from the high statistical significance of the EPIC data resulting from the unusually long observation. The outcome promises further revelations of the dynamical structure of AGN winds in a new era of high-resolution hard X-ray spectroscopy, heralded with the near-future launch of *Astro-H*.

ACKNOWLEDGEMENTS

XMM–Newton is a space science mission developed and operated by the European Space Agency. We acknowledge the excellent work of ESA staff in Madrid in planning and conducting the *XMM–Newton* observations. The UK Science and Technology Facilities Council funded the post-doctoral research assistantship of AL. We acknowledge the continued cooperation with the Leicester theory group led by Andrew King. The present text has benefited significantly in clarity from several constructive suggestions from the anonymous referee.

REFERENCES

Arnaud K. A., 1996, in Jacoby G. H., Barnes J., eds, ASP Conf. Ser. Vol. 101, Astronomical Data Analysis Software and Systems V. Astron. Soc. Pac., San Francisco, p. 17

Bentz M. C., Peterson B. M., Pogge R. W., Vestergaard M., 2009, ApJ, 694, 166

Garcia J., Dauser T., Reynolds C. S., Kallman T. R., McClintock J. E., Wilms J., Eikmann W., 2013, ApJ, 768, 146

Gofford J., Reeves J. N., Tombesi T., Braito V., Turner T. J., Miller L., Cappi M., 2013, MNRAS, 430, 60

Kallman T., Liedahl D., Osterheld A., Goldstein W., Kahn S., 1996, ApJ, 465, 994
Kaspi S., Smith P. S., Netzer H., Maoz D., Jannuzi B. T., Giveon U., 2000, ApJ, 533, 631
King A. R., Pounds K. A., 2015, ARA&A, 53, 115
King A. R., Pringle J., 2006, MNRAS, 373, 90
Lobban A. P., Vaughan S., Pounds K., Reeves J. N., 2016, MNRAS, 457, 38
Marziani P., Sulentic J. W., Dultzin-Hacyan D., Clavani M., Moles M., 1996, ApJS, 104, 37
Murphy E. M., Lockman F. J., Laor A., Elvis M., 1996, ApJS, 105, 369
Nandra K., Pounds K. A., 1994, MNRAS, 268, 405
Pounds K. A., 2014a, Space Sci. Rev., 183, 339
Pounds K. A., 2014b, MNRAS, 437, 3221
Pounds K. A., King A. R., 2013, MNRAS, 433, 1369
Pounds K. A., Page K. L., 2006, MNRAS, 360, 1123
Pounds K. A., Reeves J. N., 2009, MNRAS, 397, 249
Pounds K. A., Vaughan S., 2011, MNRAS, 415, 2379
Pounds K. A., Reeves J. N., King A. R., Page K. L., O'Brien P. T., Turner M. J. L., 2003, MNRAS, 345, 705
Pounds K. A., Lobban A., Reeves J. N., Costa M., Vaughan S., 2015, MNRAS, submitted
Reeves J., Done C., Pounds K., Terashima Y., Hayashida K., Anabuki N., Uchino M., Turner M., 2008, MNRAS, 385, L108
Strueder L. et al., 2001, A&A, 365, L18
Tombesi F., Cappi M., Reeves J. N., Palumbo G. C., Yaqoob T., Braito V., Dadina M., 2010, ApJ, 742, 44
Tombesi F., Cappi M., Reeves J. N., Palumbo G. C., Braito V., Dadina M., 2011, A&A, 521, A57
Zoghbi A. et al., 2015, ApJ, 799, L24

This paper has been typeset from a TEX/LATEX file prepared by the author.